# Variations in H2O+/H2O ratios toward massive star-forming regions

Wyrowski, F.; van der Tak, F.; Herpin, F.; Baudry, A.; Bontemps, S.; Chavarria, L.; Frieswijk, W.; Jacq, T.; Marseille, M.; Shipman, R.

*Published in:*
Astronomy & astrophysics

*DOI:*
10.1051/0004-6361/201015110

A&A 521, L34 (2010)
DOI: 10.1051/0004-6361/201015110


*Herschel/HIFI: first science highlights*

Astronomy & Astrophysics
Special feature

Letter to the Editor

# Variations in $H_2O^+/H_2O$ ratios toward massive star-forming regions*

F. Wyrowski[1], F. van der Tak[2,3], F. Herpin[4], A. Baudry[4], S. Bontemps[4], L. Chavarria[4], W. Frieswijk[3], T. Jacq[4], M. Marseille[2], R. Shipman[2], E. F van Dishoeck[5,6], A. O. Benz[7], P. Caselli[8], M. R. Hogerheijde[6], D. Johnstone[9,10], R. Liseau[11], R. Bachiller[12], M. Benedettini[13,14], E. Bergin[14], P. Bjerkeli[11], G. Blake[15], J. Braine[4], S. Bruderer[7], J. Cernicharo[16], C. Codella[13], F. Daniel[17,18], A. M. di Giorgio[13], C. Dominik[19], S. D. Doty[20], P. Encrenaz[21], M. Fich[22], A. Fuente[12], T. Giannini[13], J. R. Goicoechea[16], Th. de Graauw[23], F. Helmich[2], G. J. Herczeg[5], J. K. Jørgensen[24], L. E. Kristensen[6], B. Larsson[25], D. Lis[15], C. McCoey[22], G. Melnick[26], B. Nisini[13], M. Olberg[11], B. Parise[1], J. C. Pearson[27], R. Plume[28], C. Risacher[2], J. Santiago[12], P. Saraceno[13], M. Tafalla[12], T. A. van Kempen[26], R. Visser[6], S. Wampfler[7], U. A. Yıldız[6], J. H. Black[11], E. Falgarone[17], M. Gerin[17], P. Roelfsema[2], P. Dieleman[2], D. Beintema[2], A. De Jonge[2], N. Whyborn[23], J. Stutzki[29], and V. Ossenkopf[29]

*(Affiliations are available on page 5 of the online edition)*

Received 31 May 2010 / Accepted 19 July 2010

**ABSTRACT**

Early results from the *Herschel* Space Observatory revealed the water cation $H_2O^+$ to be an abundant ingredient of the interstellar medium. Here we present new observations of the $H_2O$ and $H_2O^+$ lines at 1113.3 and 1115.2 GHz using the *Herschel* Space Observatory toward a sample of high-mass star-forming regions to observationally study the relation between $H_2O$ and $H_2O^+$. Nine out of ten sources show absorption from $H_2O^+$ in a range of environments: the molecular clumps surrounding the forming and newly formed massive stars, bright high-velocity outflows associated with the massive protostars, and unrelated low-density clouds along the line of sight. Column densities per velocity component of $H_2O^+$ are found in the range of $10^{12}$ to a few $10^{13}$ cm$^{-2}$. The highest $N(H_2O^+)$ column densities are found in the outflows of the sources. The ratios of $H_2O^+/H_2O$ are determined in a range from 0.01 to a few and are found to differ strongly between the observed environments with much lower ratios in the massive (proto)cluster envelopes (0.01−0.1) than in outflows and diffuse clouds. Remarkably, even for source components detected in $H_2O$ in emission, $H_2O^+$ is still seen in absorption.

**Key words.** ISM: clouds – ISM: molecules – submillimeter: ISM – stars: formation

## 1. Introduction

One of the unique ESA *Herschel* Space Observatory (Pilbratt et al. 2010) science fields is the observation of thermal lines of interstellar water and other hydrides. Hydrides have small reduced masses, so their rotational lines lie at short submillimeter wavelengths, which are almost unobservable from the ground (Phillips & Vastel 2003). Early results from the first months of observations show the scientific potential of these studies (e.g. van der Tak et al. 2010, for water in a massive star-forming region). Interestingly, these early results also revealed the water cation $H_2O^+$, which was seen by *Herschel* for the first time, as an abundant ingredient of the interstellar medium (Ossenkopf et al. 2010; Gerin et al. 2010). The ortho ground-state line of $H_2O^+$ was even detected in external galaxies and found to be stronger than the para ground-state water line (Weiss et al. 2010; Van der Werf et al. 2010). These early results indicate that $H_2O^+$ originates mainly from low-density gas of diffuse interstellar clouds.

Within the "Water In Star-forming regions with *Herschel* (WISH)" (Van Dishoeck et al., in prep.) *Herschel* key program, a sample of about 20 massive star-forming regions (SFR) covering a wide range of evolutionary stages is observed in a variety of water lines. One of the $H_2O^+$ ortho ground-state doublet lines lies close in frequency to the $H_2O$ para ground-state line and is observed as well. This allows us to present here a detailed comparison of water and ionized water column densities in a larger sample of sources to study relative abundance variations of $H_2O^+$ and $H_2O$ in different interstellar environments.

## 2. Observations and data reduction

The sources were observed with the Heterodyne Instrument for the Far-Infrared (HIFI, de Graauw et al. 2010) onboard the *Herschel* Space Observatory (Pilbratt et al. 2010) on 2010 March 3−5 and April 17. Double-beam switch observations (throw of 2.5 arcmin) have been performed in the double sideband mode using the 4b receiver band. The pointing coordinates of the observed sample are given in Table 1. Data were taken in two polarizations with the acousto-optical wide band spectrometer (WBS), which covers 4−8 GHz in four

* *Herschel* is an ESA space observatory with science instruments provided by European-led Principal Investigator consortia and with important participation from NASA.

**Table 1.** Sources observed in the 1110 GHz setup.

| Source | Ra (J2000) (h m s) | Dec (° ′ ″) | $V_{\rm lsr}$ (km s$^{-1}$) | $L_{\rm bol}$ ($L_\odot/10^4$) |
|---|---|---|---|---|
| AFGL 2591 | 20 29 24.7 | +40 11 19 | −5.5 | 2.0 |
| DR21(OH) | 20 39 00.8 | +42 22 48 | −4.5 | 1.7 |
| G29.96−0.02 | 18 46 03.8 | −02 39 22 | +98.7 | 12 |
| G31.41+0.31 | 18 47 34.3 | −01 12 46 | +98.8 | 18 |
| G34.26+0.15 | 18 53 18.6 | +01 14 58 | +57.2 | 28 |
| NGC 7538-IRS1 | 23 13 45.3 | +61 28 10 | −57.4 | 20 |
| W3-IRS5 | 02 25 40.6 | +62 05 51 | −38.4 | 17 |
| W33A | 18 14 39.1 | −17 52 07 | +37.5 | 1.0 |
| W43-MM1 | 18 47 47.0 | −01 54 28 | +98.8 | 2.3 |
| W51N E1 | 19 23 40.0 | +14 30 51 | +59.0 | 10–100 |

sub-bands, each approximately 1.1 GHz wide. Its Nyquist resolution is approximately 1.1 MHz (0.30 km s$^{-1}$). Four species have been observed simultaneously with the WBS: p-$H_2O$ (1113.3 GHz, USB) and p-$H_2{}^{18}O$ $1_{11}$−$0_{00}$ (1101.7 GHz, LSB), $^{13}$CO 10−9 (1101.3 GHz, LSB), and o-$H_2O^+$ $1_{11}$−$0_{00}$ (1115.2 GHz for the strongest HF component, USB).

The system temperatures for our data were around 350 K. Integration time was 601 s. Calibration of the raw data onto $T_{\rm A}$ scale was performed by the in-orbit system (Roelfsema et al. 2010); the conversion to $T_{\rm MB}$ was done with a beam efficiency of 0.7. The *Herschel* full-beam-at-half-maximum at this frequency was assumed to be the theoretical one (20″). Currently, the flux scale is accurate to 5%. An rms of 90 mK has been reached.

Data calibration was performed in the *Herschel* interactive processing environment (HIPE) version 2.8. The velocity uncertainty in the current version of the pipeline is up to 2 km s$^{-1}$, depending on target direction and observation epoch. Further analysis was done within the CLASS package. After inspection, the data from the two polarizations were averaged together. The continuum level in the data was divided by two, because the original calibration was done for the line emission originating from only one receiver sideband.

## 3. Results

In Fig. 1 the DSB WBS spectrum towards G34.26+0.15 is shown as a typical example for the data that are analyzed in this study. $H_2O^+$ is detected in all sources except NGC 7538 IRS1 and in all cases seen in absorption, similar to the previous detections (Ossenkopf et al. 2010; Gerin et al. 2010). $H_2O$ and $H_2^{18}O$ on the other hand show in many cases both absorption and emission line components. Many sources show several velocity components owing to absorption from diffuse clouds from different spiral arms on the lines of sight (LOS), which complicates the interpretation of the $H_2O^+$ spectra because of its complex hyperfine structure (HFS, see Strahan et al. 1986; Mürtz et al. 1998, for details). Several sources show saturated $H_2O$ absorption down to the 0 K level (e.g. Figs. 1–3), demonstrating that the continuum level in the spectra is measured reliably and that the sideband gain ratio is 1. This is especially important because most of the analysis is based on the detected absorption features for which the line-to-continuum ratio is the relevant observing parameter. Most of the sources show broad wing emission ($\Delta V$ > 10 km s$^{-1}$) as an indication of powerful outflows, in $H_2O$ mostly seen in emission, while in $H_2O^+$ outflows are detected as broad (due to the blended HFS) blueshifted absorption features in front of the strong dust continuum emission.

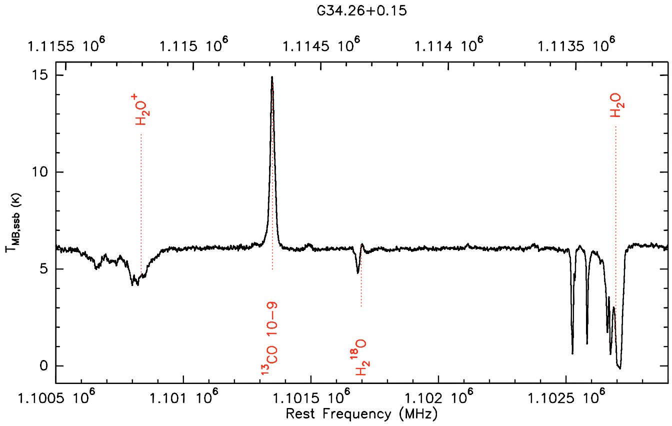


**Fig. 1.** Example DSB spectrum at 1110 GHz towards G34.26 showing all lines covered in this spectral setup at the $V_{\rm LSR}$ of the source. The redshifted $H_2O$ and $H_2O^+$ features are caused by the line-of-sight absorption components. The lower and upper scales give the LSB and USB frequency scales, respectively.

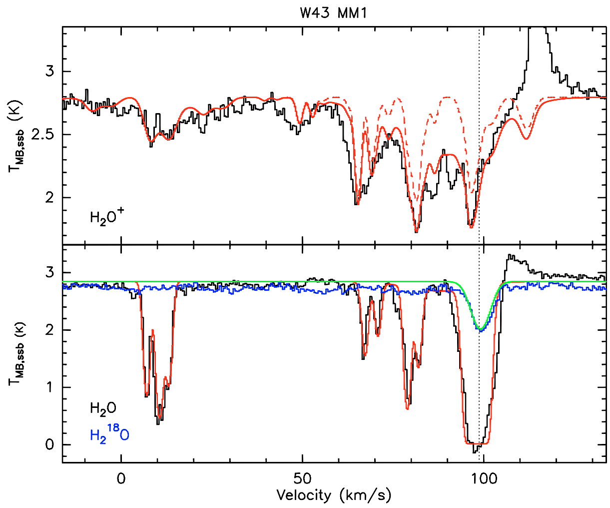


**Fig. 2.** XCLASS fits to the water (*lower panel*) and water ion line profiles (*upper panel*) in W43 MM1 shown in red solid lines. The fit to the $H_2^{18}O$ line (blue spectrum) is shown in green. An $H_2O^+$ fit without a broad outflow component is shown with red dots. The systemic velocity of the source is indicated by a dotted line. The strong emission line in the $H_2O^+$ spectrum is $^{13}$CO (10−9) from the other sideband.

## 4. Analysis

Because all lines for a given source are observed simultaneously in the DSB spectra, they will only have a small relative error in their intensities and velocities independent of the calibration. Here, the rest frequencies from Mürtz et al. (1998) are used, which have a quoted accuracy of 2 MHz. A comparison of the $H_2O$ and $H_2O^+$ velocities from LOS absorption features shows a small scatter of ±2 km s$^{-1}$, hence the resulting accuracy of the measured $H_2O^+$ velocities is sufficient to associate them with known velocity components of the observed sources.

To separate the various and often blended velocity components and the $H_2O^+$ HFS, we used the XCLASS fitting tool (Comito et al. 2005, and references therein), which allows us to obtain multi-component LTE fits of emission and absorption components and which takes the HFS – which extends over 40 km s$^{-1}$ (Mürtz et al. 1998) – into account. The input parameters for the fits are the excitation temperature, column density,

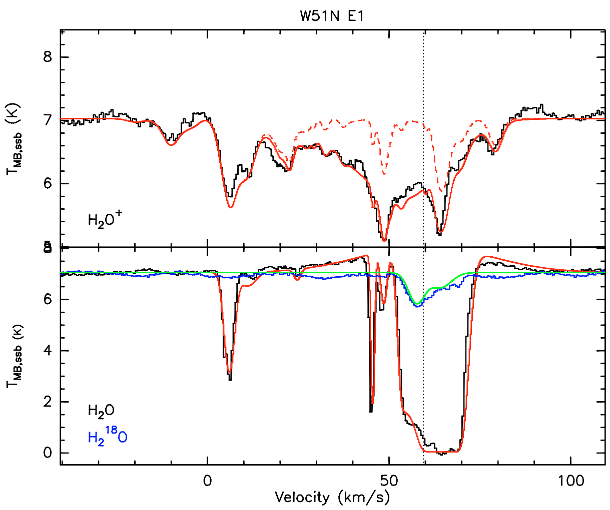


**Fig. 3.** Same as Fig. 2 for W51N E1.

**Table 2.** $H_2O$, $H_2^{18}O$ and $H_2O^+$ fit results of velocity components associated with the massive star-forming clumps W43 and W51 shown in Figs. 2 and 3.

| Mol./Source | $T_{ex}$ (K) | $N/10^{12}$ ($cm^{-2}$) | $\Delta V$ (km $s^{-1}$) | $V_{lsr}$ (km $s^{-1}$) |
|---|---|---|---|---|
| $H_2O$/W43 MM1 | 2.7 | 6.0 | 2.0 | 7.0 |
| | 2.7 | 9.0 | 2.0 | 10.5 |
| | 2.7 | 5.0 | 2.0 | 13.0 |
| | 2.7 | 3.0 | 2.0 | 66.5 |
| | 2.7 | 2.0 | 2.0 | 70.0 |
| | 2.7 | 7.5 | 2.0 | 78.0 |
| | 2.7 | 3.5 | 2.0 | 81.0 |
| | 5.0 | 3.0 | 20.0 | 87.0 |
| | 5.0 | 200.0 | 4.0 | 97.0 |
| $H_2^{18}O$ | 5.0 | 5.0 | 6.0 | 99.0 |
| $H_2O^+$ | 2.7 | 3.0 | 4.0 | 8.0 |
| | 2.7 | 1.2 | 4.0 | 11.5 |
| | 2.7 | 1.5 | 4.0 | 14.0 |
| | 2.7 | 3.0 | 2.0 | 64.5 |
| | 2.7 | 2.0 | 2.0 | 68.0 |
| | 2.7 | 1.0 | 2.0 | 78.0 |
| | 2.7 | 3.0 | 2.0 | 80.5 |
| | 5.0 | 6.0 | 4.0 | 96.0 |
| | 5.0 | 15.0 | 20.0 | 87.0 |
| $H_2O$/W51N E1 | 2.7 | 6.0 | 3.0 | 6.0 |
| | 2.7 | 1.0 | 5.0 | 11.0 |
| | 2.7 | 0.3 | 2.0 | 24.5 |
| | 2.7 | 3.5 | 1.0 | 45.0 |
| | 2.7 | 1.5 | 2.0 | 48.0 |
| | 5.0 | 400.0 | 5.0 | 57.5 |
| | 50.0 | 100.0 | 40.0 | 59.5 |
| | 2.7 | 250.0 | 7.0 | 64.0 |
| $H_2^{18}O$ | 5.0 | 3.0 | 5.0 | 57.5 |
| | 2.7 | 1.5 | 7.0 | 64.0 |
| $H_2O^+$ | 2.7 | 6.0 | 5.0 | 6.0 |
| | 2.7 | 2.0 | 5.0 | 11.0 |
| | 2.7 | 0.5 | 2.0 | 22.5 |
| | 2.7 | 0.3 | 1.0 | 45.0 |
| | 2.7 | 1.0 | 2.0 | 48.0 |
| | 5.0 | 17.0 | 20.0 | 50.0 |
| | 5.0 | 0.3 | 5.0 | 57.5 |
| | 2.7 | 4.0 | 4.0 | 64.0 |

source size, source velocity and velocity width. For the absorption components, a background brightness temperature of 15−25 K was derived from the measured continuum temperatures assuming source sizes as given in Table 2.

The $H_2O$ absorption components with high velocity offsets, which are likely diffuse LOS clouds, were fitted with an excitation temperature of 2.7 K. However, the diffuse Galactic background radiation might increase the excitation temperatures of the submillimeter lines to values of about 5 K. For absorption components that are likely associated with the massive SFRs we used a fixed value of 5 K, which is clearly below the background temperature, to get an absorption in the fit. However, the corresponding column densities for temperatures below 10 K depend only weakly on the assumed $T_{EX}$. For the emission components we used a fixed value of 50 K. The source size is assumed to be much bigger than the beam. Only for the 57.5 km $s^{-1}$ component toward W51N E1 a size of 35″ is assumed. Judging from its strong $H_2^{18}O$ absorption, it has a very high $H_2O$ optical depth, but still does not absorb the continuum down to 0 K and therefore requires a filing factor smaller than one. For the column density calculations we used an ortho-to-para ratio of 3:1 for $H_2O^+$.

The fit results obtained for $H_2O$ were used as the starting point to fit the $H_2O^+$ spectra, which are more complex owing to the $H_2O^+$ HFS. because no emission is seen in $H_2O^+$, we changed any component seen in emission in $H_2O$ into an absorption component for $H_2O^+$ by lowering its excitation temperature to 5 K. The physical parameters for each component were then fine-tuned to fit the observed $H_2O^+$ spectra. In cases where the corresponding component was not detected in $H_2O^+$, the highest column density consistent with a non-detection was chosen to derive an upper limit. In a few cases, the observed $H_2O$ components were not sufficient to account for all the $H_2O^+$ absorption. In Fig. 2 e.g. there is no indication of an $H_2O$ outflow component and the blue-shifted LOS absorptions are quite narrow, while the $H_2O^+$ absorption is very broad, even considering its HFS, so that an additional blueshifted, broad "outflow" component ($\Delta V > 10$ km $s^{-1}$) was added to reproduce the observed $H_2O^+$ spectrum.

Two examples for the resulting fits are shown in Figs. 2 and 3. The corresponding fit parameters for these sources are given in Table 2. The range in $N(H_2O^+)$ of $10^{12}$ to a few $10^{13}$ $cm^{-2}$ is much smaller than the range in $N(H_2O)$ of a few $10^{12}$ to several $10^{14}$ $cm^{-2}$. Similar results are obtained for other sources in our sample and will be discussed elsewhere and in the following section.

## 5. Discussion and conclusions

An overview of the fit results is shown in Fig. 4, in which we plot for each velocity component the corresponding $H_2O$ and $H_2O^+$ column densities. Some of the lower column densities are upper limits while some of the high $H_2O$ column densities are lower limits because of the saturation in the $H_2O$ absorption lines. In these cases the true column density, estimated from the observed $H_2^{18}O$ lines and assuming a $^{16}O/^{18}O$ ratio in the range from 250−560 (Wilson & Rood 1994) will be higher by up to a factor 5. Figure 4 shows that compared to the properties of diffuse clouds (see also Gerin et al. 2010; Ossenkopf et al. 2010; Weiss et al. 2010), in which $N(H_2O^+)$ is closer to $N(H_2O)$, significantly higher $N(H_2O)/N(H_2O^+)$ is found for velocity components likely originating from the envelopes and bright high-velocity outflows of the massive star-forming clumps. Even in the outflows and envelopes of the massive star-forming regions there is still a variation of $N(H_2O^+)$. The highest $N(H_2O^+)$ column densities are found in the outflows.

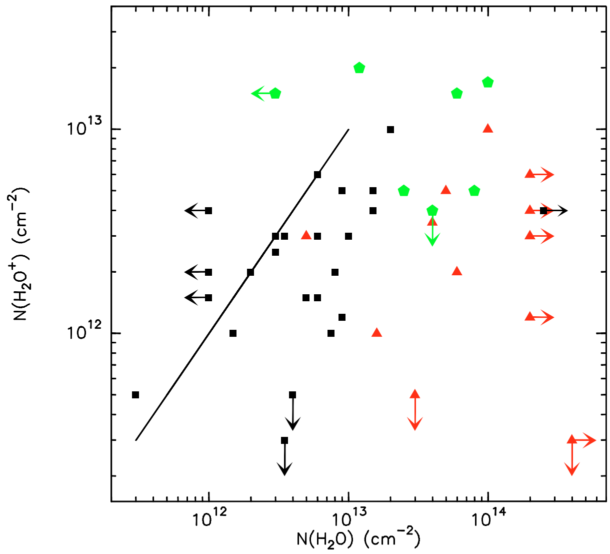


**Fig. 4.** Comparison of $H_2O$ and $H_2O^+$ column densities of different line components in the spectra: the black squares give diffuse lines of sight, red triangles the envelopes of the massive star-forming clumps, and green filled dots the outflow components ($\Delta V > 10$ km s$^{-1}$). As a reference, the solid line shows $N(H_2O^+) = N(H_2O)$. Some of the low (high) column densities are upper (lower) limits and are indicated by arrows.

After the first indication that $H_2O^+$ is present in the outflow of DR21 (Ossenkopf et al. 2010), it is clearly detected here in several outflows. Some outflows are even more prominent in $H_2O^+$ than in $H_2O$ (e.g. outflow components above the diffuse cloud region of Fig. 4), although in some cases it is difficult to disentangle the blueshifted outflow and spiral arm absorption.

In Fig. 4 one cloud treated in the literature as diffuse LOS cloud toward W51 (64 km s$^{-1}$ component, Sollins et al. 2004) has a high $H_2O/H_2O^+$ ratio of 50, which indicates that it might rather be associated with the W51 clump envelope. Strong ortho-water absorption of this component was already seen with SWAS by Neufeld et al. (2002). Hence the $H_2O/H_2O^+$ ratio might be useful for the classification of absorption components.

A key result from our observation of a quite significant sample is that $H_2O^+$ is always seen in absorption, even when originating from outflows or envelopes, in which water is seen in several cases in emission. This finding might point to the origin of $H_2O^+$ from low-density environments, but alternatively, because $H_2O^+$ is a highly reactive molecular ion that reacts rapidly with $H_2$ and electrons, inelastic collisions are very ineffective at exciting it into emission, regardless of the density.

The new detections of $H_2O^+$ toward Galactic star-forming regions presented here together with the recent detection of $OH^+$ from the ground (Wyrowski et al. 2010) and from space (Gerin et al. 2010; Benz et al. 2010; Bruderer et al. 2010) are an important confirmation of the gas-phase route to water. The $H_2O^+$ lines are stronger than the $H_3O^+$ lines in the same sources (some of is caused by differences in spectroscopic properties), which is surprising, because $H_2O^+$ is expected to react fast with $H_2$ into $H_3O^+$, which recombines with electrons to produce $H_2O$. This puzzle is even more pronounced in recent *Herschel*/HIFI observations in diffuse clouds (Gerin et al. 2010) and active galactic nuclei (Weiss et al. 2010), where $H_2O^+$ is even more abundant than $H_2O$ itself. While for AGN strong X-ray and/or UV radiation is likely to dominate the chemistry (Van der Werf et al. 2010), environments without radiation sources require other solutions. One solution might be that in the outer envelopes of the massive SFRs $H_2O$ is freezing out onto grains whereas – in the case of positively charged grains – $H_2O^+$ is much less affected by freeze-out.

The main destruction routes of $H_2O^+$ are dissociative recombination (into OH) and reaction with $H_2$ (into $H_3O^+$ and $H_2O$). The high $H_2O^+/H_2O$ ratio observed in the diffuse components implies that the first channel is faster than the second. In gas where all hydrogen is in molecular form, the electron fraction is $10^{-4}$ at most when all carbon is ionized, which is not enough to make recombination faster than the reaction with $H_2$. Our observations therefore imply that a significant fraction of the hydrogen in the outflows is in atomic form. The same conclusion applies to diffuse clouds, where UV radiation causes partial dissociation of $H_2$ (Gerin et al. 2010), and also to AGN, where X-rays are responsible (Van der Werf et al. 2010). For molecular outflows the most likely mechanism to dissociate $H_2$ is by fast (J-type) shocks. The required shock velocities of 30–40 km s$^{-1}$ are easily reached in the powerful outflows of the sources.

Models of dense PDRs (e.g. Sternberg & Dalgarno 1995) predict $OH^+ + H_2 \rightarrow H_2O^+$. In the outflow-walls scenario (Bruderer et al. 2009) this leads to a thin PDR layer along the outflow wall, where FUV heats and ionizes the gas. New modeling of Bruderer et al. (2010, submitted) of hydrides including $H_2O^+$ predicts the abundance of $H_2O^+$ to be enhanced by four orders of magnitude along the outflow compared to the envelope, which then could explain the high column densities of $H_2O^+$ in the outflow components.

*Acknowledgements.* The XCLASS program (http://www.astro.uni-koeln.de/projects/schilke/XCLASS) was used, which accesses the CDMS (http://www.cdms.de) and JPL (http://spec.jpl.nasa.gov) molecular data bases. HIFI has been designed and built by a consortium of institutes and university departments from across Europe, Canada and the United States under the leadership of SRON Netherlands Institute for Space Research, Groningen, The Netherlands and with major contributions from Germany, France and the US. Consortium members are: Canada: CSA, U. Waterloo; France: CESR, LAB, LERMA, IRAM; Germany: KOSMA, MPIfR, MPS; Ireland, NUI Maynooth; Italy: ASI, IFSI-INAF, Osservatorio Astrofisico di Arcetri- INAF; Netherlands: SRON, TUD; Poland: CAMK, CBK; Spain: Observatorio Astronomico Nacional (IGN), Centro de Astrobiologia (CSIC-INTA). Sweden: Chalmers University of Technology – MC2, RSS & GARD; Onsala Space Observatory; Swedish National Space Board, Stockholm University – Stockholm Observatory; Switzerland: ETH Zurich, FHNW; USA: Caltech, JPL, NHSC. HCSS/HSpot/HIPE is a joint development (are joint developments) by the *Herschel* Science Ground Segment Consortium, consisting of ESA, the NASA *Herschel* Science Center, and the HIFI, PACS and SPIRE consortia. We would like to thank the referee, Christian Henkel, for a thorough review of the manuscript and helpful comments.

## References

Benz, A. O., Bruderer, S., van Dishoeck, E. F., et al. 2010, A&A, 521, L35
Bruderer, S., Benz, A. O., Bourke, T. L., & Doty, S. D. 2009, A&A, 503, L13
Bruderer, S., Benz, A. O., van Dishoeck, E. F., et al. 2010, A&A, 521, L44
Comito, C., Schilke, P., Phillips, T. G., et al. 2005, ApJS, 156, 127
de Graauw, Th., Helmich, F. P., Phillips, T. G., et al. 2010, A&A, 518, L6
Gerin, M., de Luca, M., Black, J., et al. 2010, A&A, 518, L110
Mürtz, P., Zink, L. R., Evenson, K. M., & Brown, J. M. 1998, J. Chem. Phys., 109, 9744
Neufeld, D. A., Kaufman, M. J., Goldsmith, P. F., Hollenbach, D. J., & Plume, R. 2002, ApJ, 580, 278
Ossenkopf, V., Müller, H. S. P., Lis, D. C., et al. 2010, A&A, 518, L111
Phillips, T. G., & Vastel, C. 2003, in SFChem 2002: Chemistry as a Diagnostic of Star Formation, ed. C. L. Curry, & M. Fich, 3
Pilbratt, G. L., Riedinger, J. R., Passvogel, T., et al. 2010, A&A, 518, L1
Roelfsema, P. R., Helmich, F. P., Teyssier, D., et al. 2010, A&A, submitted
Sollins, P. K., Zhang, Q., & Ho, P. T. P. 2004, ApJ, 606, 943
Sternberg, A., & Dalgarno, A. 1995, ApJS, 99, 565
Strahan, S. E., Mueller, R. P., & Saykally, R. J. 1986, J. Chem. Phys., 85, 1252
van der Tak, F. F. S., Marseille, M. G., Herpin, F., et al. 2010, A&A, 518, L107
Van der Werf, P. P., Isaak, K. G., Meijerink, R., et al. 2010, A&A, 518, L42
Weiss, A., Requena-Torres, M. A., Güsten, R., et al. 2010, A&A, 521, L1
Wilson, T. L., & Rood, R. 1994, ARA&A, 32, 191
Wyrowski, F., Menten, K. M., Güsten, R., & Belloche, A. 2010, A&A, 518, A26

[1] Max-Planck-Institut für Radioastronomie, Auf dem Hügel 69, 53121 Bonn, Germany
e-mail: wyrowski@mpifr-bonn.mpg.de
[2] SRON Netherlands Institute for Space Research, PO Box 800, 9700 AV, Groningen, The Netherlands
[3] Kapteyn Astronomical Institute, University of Groningen, PO Box 800, 9700 AV, Groningen, The Netherlands
[4] Université de Bordeaux, Laboratoire d'Astrophysique de Bordeaux, France; CNRS/INSU, UMR 5804, Floirac, France
[5] Max Planck Institut for Extraterestrische Physik, Garching, Germany
[6] Leiden Observatory, Leiden University, PO Box 9513, 2300 RA Leiden, The Netherlands
[7] Institute of Astronomy, ETH Zurich, 8093 Zurich, Switzerland
[8] School of Physics and Astronomy, University of Leeds, Leeds LS2 9JT, UK
[9] National Research Council Canada, Herzberg Institute of Astrophysics, 5071 West Saanich Road, Victoria, BC V9E 2E7, Canada
[10] Department of Physics and Astronomy, University of Victoria, Victoria, BC V8P 1A1, Canada
[11] Department of Radio and Space Science, Chalmers University of Technology, Onsala Space Observatory, 439 92 Onsala, Sweden
[12] IGN Observatorio Astronómico Nacional, Apartado 1143, 28800 Alcalá de Henares, Spain
[13] INAF - Istituto di Fisica dello Spazio Interplanetario, Area di Ricerca di Tor Vergata, via Fosso del Cavaliere 100, 00133 Roma, Italy
[14] Department of Astronomy, The University of Michigan, 500 Church Street, Ann Arbor, MI 48109-1042, USA
[15] California Institute of Technology, Division of Geological and Planetary Sciences, MS 150-21, Pasadena, CA 91125, USA
[16] Department of Astrophysics, CAB, INTA-CSIC, Crta Torrejón a Ajalvir km 4, 28850 Torrejón de Ardoz, Spain
[17] Observatoire de Paris-Meudon, LERMA UMR CNRS 8112, 5 place Jules Janssen, 92195 Meudon Cedex, France
[18] Department of Molecular and Infrared Astrophysics, Consejo Superior de Investigaciones Cientificas, C/ Serrano 121, 28006 Madrid, Spain
[19] Astronomical Institute Anton Pannekoek, University of Amsterdam, Kruislaan 403, 1098 SJ Amsterdam, The Netherlands
[20] Department of Physics and Astronomy, Denison University, Granville, OH, 43023, USA
[21] LERMA and UMR 8112 du CNRS, Observatoire de Paris, 61 Av. de l'Observatoire, 75014 Paris, France
[22] University of Waterloo, Department of Physics and Astronomy, Waterloo, Ontario, Canada
[23] Atacama Large Millimeter/Submillimeter Array, Joint ALMA Office, Santiago, Chile
[24] Centre for Star and Planet Formation, Natural History Museum of Denmark, University of Copenhagen, Øster Voldgade 5-7, 1350 Copenhagen, Denmark
[25] Department of Astronomy, Stockholm University, AlbaNova, 106 91 Stockholm, Sweden
[26] Harvard-Smithsonian Center for Astrophysics, 60 Garden Street, MS 42, Cambridge, MA 02138, USA
[27] Jet Propulsion Laboratory, California Institute of Technology, Pasadena, CA 91109, USA
[28] Department of Physics and Astronomy, University of Calgary, Calgary, T2N 1N4, AB, Canada
[29] Physikalisches Institut, Universität zu Köln, Zülpicher Str. 77, 50937 Köln, Germany